Evolution in Time of a Gold−Zirconia Nanopowder at Room Temperature: Nucleation Growth of Gold Nanoparticles

M. Isa, J. Ch. Valmalette,* Ch. Muller, and Ch. Leroux

Laboratoire Matériaux et Microélectronique de Provence (L2MP), UMR CNRS 6137, Université du Sud Toulon Var, BP 20132, 83957 La Garde Cedex, France

Received July 30, 2004

This work exposes the study of the nucleation and growth of gold nanoparticles at a temperature of 25 °C induced by the spontaneous oxidation at room temperature of the ZrAu crystallized alloy. In this rich gold original system, the starting gold nuclei are produced by the degradation of the ZrAu crystal structure by atmospheric oxygen (selective oxidation of zirconium). The nucleation-growth mechanism has been followed by X-ray diffraction and described with the Johnson−Mehl−Avrami−Kolmogorov (JMAK) model. From the JMAK calculation and the Rietveld analysis, it has been shown that this mechanism could be decomposed in two steps: a nucleation regime followed by a thickening of the particles formed during the first step. The growth model interpretation by the Avrami analysis has been verified thanks to the study of the evolution of crystallite dimensions during 1 year at room temperature and also by transmission electron microscopy obervations. Microstructural analysis has allowed a determination of the mean size of gold nanoparticles (about 3 nm in diameter after 10 days). This association of very fine particles of ZrO_2 and Au could open plenty of perspectives in the field of catalysis sensors because of the nanosized scale.

1. Introduction

Growth of nanoparticles at room temperature from solid state has been poorly studied because of their very slow kinetics. However, the growth of nanoparticles and especially metal particles is known to occur at room temperature.[1−4]

Johnson−Mehl−Avrami−Kolmogorov analysis is applied to various research fields such as crystallization from amorphous alloys, degradation phenomena, nucleation and growth in glasses, grain growth under irradiation, and crystallization of polymers. Several techniques such as differential scanning calorimetry and differential thermal analysis,[5−7] complex impedance spectroscopy,[8] optical absorption,[9] electropolymerization, and resistivity evolution can be used to characterize oxidation and evolution of volume transformed. However, all these phenomena are usually studied at a temperature different from the ambient temperature, because of their generally very slow kinetics. For example, oxidation of amorphous Zr-based binary alloys in air and at room temperature, studied by Kimura et al.,[10] gives significant results after 7−9 years.

The theoretical understanding of the nucleation and growth mechanisms of very fine particles at room temperature is actually not well-known. Moreover, results concerning the catalysis activity of small gold nanoparticles[11,12] put the light on the necessity of this understanding for the industrial applications perspectives. As they are "nanosized", these products could be very interesting in the gas catalysis domain in providing association between nanosized noble metal clusters and nanosized transition metal oxide and, therefore, increasing the specific area available for catalysis reactions.[13,14] Indeed, the characteristics of the final products offer plenty of perspectives as catalytic powder gas sensors, the association ZrO_2−Au being well-known as catalytic activators of oxidative reaction for gases conversion.[15−17]

ZrAu is extremely reactive and is spontaneously oxidized in air and at room temperature and atmospheric pressure. The oxidation kinetics is linear, with an oxide layer growth of 2 μm/day, and very fast compared with the usual room-temperature corrosion processes. Products of this reaction are gold and zirconia nanoparticles.[18,19]

* Corresponding author.

(1) Gertsman, V. Y.; Birringer, R. *Scr. Metall. Mater.* **1994**, *30*, 577−581.
(2) Weissmüller, J.; Löffler, J.; Kleber, M. *Proc. 2nd Conf. On Nanostructured Materials, Nanostruct. Mater.* **1995**, *6*, 105.
(3) Günther, B.; Kumpmann, A.; Kunze, H.-D. *Scr. Metall. Mater*. **1992**, *27*, 833.
(4) Löffler, J. Diploma Thesis. Universität des Saarlandes, 1994.
(5) Smith, G. W. *Scr. Metall. Mater.* **1994**, *31* (3), 357.
(6) Malek, J.; Matsuda, S.; Watanabe, A.; Ikegami, T.; Mitsuhashi, T.; *Thermochim. Acta* **1995**, *267*, 181.
(7) Li, W.; Mitchell, B. S. *J. Non-Cryst. Solids* **1999**, *255*, 199.
(8) Villain, S.; Pischedda, M. H.; Nigrelli, E.; Godiart, F.; Gavarri, J. R. *Corros. Sci.* **2002**, *44* (4), 657
(9) Rao, P.; Doremus, R. *J. Non-Cryst. Solids* **1996**, *203*, 202.
(10) Kimura, H. M.; Asami, K.; Inoue, A.; Masumoto, T. *Corros. Sci.* **1993**, *35* (5−8), 909−915.
(11) Bond, G. C.; Thompson, D. T. *Catal. Rev.—Sci. Eng.* **1999**, *41* (3−4), 319.
(12) Heiz, U.; Sanchez, A.; Abbet, S.; Schneider, W.-D. *Eur. Phys. J. D* **1999**, *9*, 35.
(13) Edelstein, A. S.; Cammarata, R. C. *Nanomaterials: synthesis, properties and applications*; Institute Of Physics Publishing (IOP): Bristol and Philadelphia, 1998; Chapter 12.
(14) Campbell, C. T.; Parker, S. C.; Starr, D. E. *Science* **2002**, Oct 25, 811−814.
(15) Knell, A.; Barnickel, P.; Baiker, A.; Wokaun, A. *J. Catal.* **1992**, *137*, 306−321.
(16) Grunwaldt, J.-D.; Kiener, C.; Wögerbauer, C.; Baiker, A. *J. Catal.* **1999**, *181*, 223−232.
(17) Grunwaldt, J.-D.; Maciejewski, M.; Becker, O. S.; Fabrizioli, P.; Baiker, A. *J. Catal.* **1999**, *186*, 458−469.

10.1021/cm040187j CCC: $30.25
Published on Web 11/02/2005

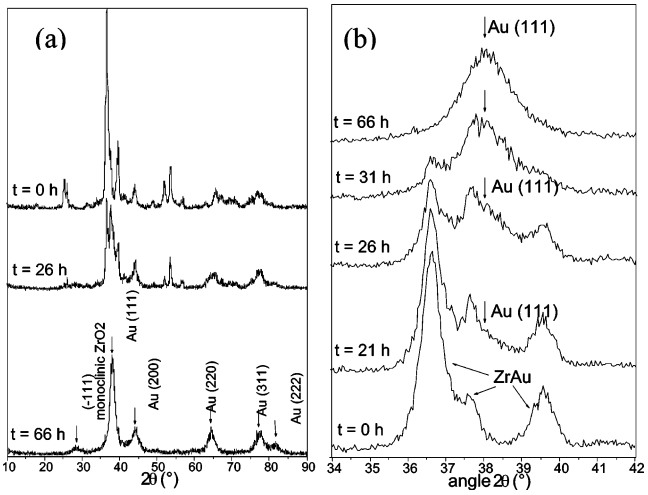

Figure 1. (a) Time-dependent evolution of the X-ray diffraction patterns over the whole investigated angular domain. All initial ZrAu peaks vanish and are replaced by Bragg peaks attributed to monoclinic zirconia and gold. (b) Evolution around the (111) gold peak position.

In this paper we have focused our attention on the overall study of the evolution of the nanopowder and on the kinetic of nucleation and growth of gold nanoparticles at room temperature. This kinetics has been followed from X-ray diffraction experiments. Morphology of nanoparticles has been observed in transmission electron microscopy (TEM). The process of degradation of the initial alloy which engenders these particles has been treated separately.[21]

We have chosen to use X-ray diffraction experiments because this technique is a non-destructive means of study and the oxidation kinetics is rapid enough that a kinetics measurement of the process can be performed.

2. Experimental Section

The ZrAu alloy was prepared by arc melting and tempering under argon flow from zirconium powder (99.8%) and gold wires (99.99%) and was obtained in an ingot form from which slices were cut. Time-dependent X-ray diffraction experiments were performed on the surfaces of these slices to characterize the diffracting domain dimensions of surface species. These studies were carried out on a Siemens D5000 diffractometer (Cu $K\alpha_{1,2}$ radiations; 2θ range, 10−110°) equipped with a back monochromator. Evolution of X-ray diffraction diagrams at room temperature shows that the primary alloy disappears progressively to form the products of reaction, that is, gold and zirconia.[21] In 3 days all the volume analyzed by X-rays is transformed, the initial peaks of the ZrAu phase vanishing in the background, whereas the Bragg peaks of gold and monoclinic zirconia exhibit a simultaneous increase (Figure 1a). Over the angular range 34−42° in 2θ, one can distinguish the progressive appearance of a diffraction line at around 38° corresponding to the (111) Au Bragg reflection, whereas the group of peaks of the initial ZrAu phase vanishes in the background (Figure 1b). Study has been realized on the evolution in time at room temperature of this latter gold peak.

Description of the Model Used To Describe the Nucleation-Growth Process. The isothermal three-dimensional nucleation and growth processes of particles are usually detailed by the JMAK theory. The model describes the evolution in time of the volume $V(t)$ of the new phase nucleating and growing.[22−25] The model is expressed as a ratio between $V(t)$ and the final volume V_∞ occupied by this phase when the reaction is complete: $X(t)$. In the case of spheric particles and the three-dimensional nucleation and growth mechanism, Avrami expressed $X(t)$ as follows:

$$X(t) = 1 - \exp(4\pi/3)\gamma^3 \int_0^t J(1-\tau)^3 \, d\tau \quad (1)$$

$0 \le X(t) \le 1$, that is, when $X(t) = 1$ all of the new phase has been formed, γ is the growth rate, J the nucleation rate, and τ the induction period of the process.

The general relation becomes[26−28]

$$X(t) = 1 - \exp(-kt^n) \quad (2)$$

where n is the JMAK exponent (or Avrami exponent, AE). In general, this formula remains valid for two- and one-dimensional processes by changing the AE value[22,23]

Equation 2 can be rewritten as

$$\ln\{-\ln[1 - X(t)]\} = \ln k + n \ln t \quad (3)$$

The major difficulty of this model is based on the measure of the volume of the new phase as a function of time. If we can correlate the evolution of a physical property $p(t)$ (measure of an electric current, dilatometric measurements, etc.) to the evolution of the volume of the considered phase, the fraction of the volume transformed can be expressed by the Weibull expression:[24]

$$X(t) = [p(t) - p_0]/(p_\infty - p_0) \quad (4)$$

where p_0 and p_∞ are respectively the value of the considered measurement at the beginning and at the end of the process.

This leads to the Weibull type function[29]

$$p(t) = p_\infty - (p_\infty - p_0)\exp(-kt^n) \quad (5)$$

In the case of X-ray diffraction, the integrated intensity of a diffraction peak, $I(t)$, will be proportional to $V(t)$ which is the total diffracting volume of gold analyzed by the beam in the (111) direction independently of the shape of particles[30] whereas the integral breadth of the same peak, $\beta(t)$, will be proportional to the mean size of the particles in the considered direction.[31] In the case of spherical particles, $\beta(t)$ is related to the mean volume of particles, $V_\beta(t)$, by the relation

$$V_\beta(t)/V_{\beta\infty} = D(t)^3/D_\infty{}^3 = \beta_\infty{}^3/\beta(t)^3 \quad (6)$$

Consequently, two quantities can be defined:

$$X(t) = [V(t) - V_0]/(V_\infty - V_0) \quad (7)$$

and

$$X_\beta(t) = [V_\beta(t) - V_{\beta 0}]/(V_{\beta\infty} - V_{\beta 0}) \quad (7')$$

(18) Valmalette, J. Ch.; Lomello-Tafin, M.; Galez, P.; Jorda, J.-L. Communication. Presented at 4th Int. Conf. Nanostructur. Mater., NANO'98, Stockholm, Sweden, 1998.
(19) Valmalette, J. Ch.; Isa, M.; Passard, M.; Lomello-Tafin, M. *Chem. Mater.* **2002**, *14*, 2048−2054.
(20) Isa, M.; Valmalette, J. Ch.; Muller, Ch.; Lomello-Tafin, M.; Gas, P.; Elkaïm, E. *J. Alloys Compd.* **2004**, *373* (1−2), 96−103.
(21) Valmalette, J. Ch.; Isa, M. *Chem. Mater.* **2002**, *14*, 5098−5102.
(22) Christian, J. W. The theory of transformations in metals and alloys Part 1. Pergamon Press: Elmsford, NY, 1981 (reprint).
(23) Hulbert, S. F. *J. Br. Ceram. Soc.* **1969**, 11−19.
(24) Mittemeijer, E. J. *J. Mater. Sci.* **1992**, *27*, 3977−3987.
(25) Jacobs, P. W. M.; Tompkins, F. C. Classification and Theory of Solid Reactions. In *Chemistry of Solid State*; Garner, W. E., Ed.; Butterworths/London Scientific Publication: 1953.

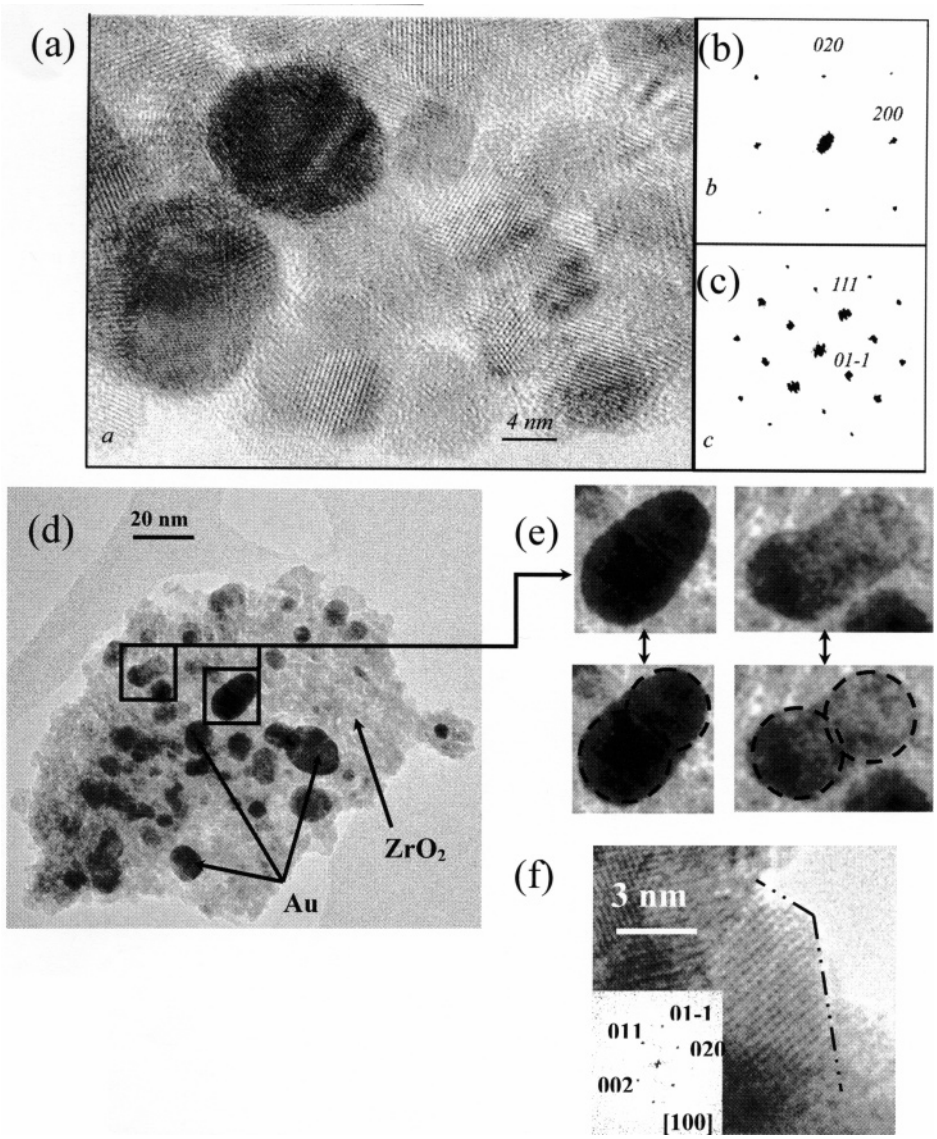

Figure 2. (a) High-resolution TEM image showing two types of nanoparticles in the Au−ZrO_2 powder after 11 months. The nearly round particles with a high contrast are gold particles. The other particles with no peculiar shapes correspond to *m*−ZrO_2 particles. (b) Fourier transform of a gold particle oriented [001]. (c) Fourier transform of a *m*−ZrO_2 particle oriented [$\bar{2}$11]. (d−e) High-resolution TEM images of one of the thinnest agglomerates. We can easily observe both populations of gold nanoparticles and the "dumbbell" characteristic shape of the biggest gold nanoparticles. This shape can be correlated to the coalescence of two particles as represented below. (f) High-resolution TEM image of a zirconia nanoparticle showing its facetted morphology.

The next step is to evaluate the value of V_0 and $V_{\beta 0}$, that is, to know if small gold nuclei (few atoms) pre-exist in the alloy when the oxidation process begins (which can constitute a pre-existing volume of gold). This information will have an important repercussion on the AE value. As we can note the absence of significant gold reflections in the initial X-ray diffractogram (Figure 2b), the initial total volume of gold can be neglected ($V_0 = 0$).

Then

$$X(t) = V(t)/V_\infty = 1 - \exp[-k(t)^n] \tag{8}$$

and

$$X_\beta(t) = V_\beta(t)/V_{\beta\infty} = 1 - \exp[-k(t)^{n_\beta}] \tag{8'}$$

where n and n_β are the mean AEs of each evolution. However, there are several ways to increase the total volume. The first is to increase the number of particles constituting this latter, and the second is to increase the mean volume of each particle $V_\beta(t)$.

3. Results

X-ray Diffraction Analysis. Following eqs 8 and 8′, $X(t)$ and $X_\beta(t)$ have been plotted and fitted (Figure 3a). The mean AEs deduced are respectively equal to $n = 2.6$ and $n_\beta = 2.56$. The weakness of a direct Avrami analysis on the ratio evolution is that it imposes an asymptotic behavior to the end of the fit. Both the linear form of $X(t)$ and the linear form of $X_\beta(t)$ have been plotted in Figure 3b following eq 2. We can see that each plot can be decomposed in two parts and that the slope break occurs approximately at the same time t_0 in both cases. Moreover, the second parts of both

(26) Avrami, M. *J. Chem. Phys.* **1939**, *7*, 1103−1112.
(27) Avrami, M. *J. Chem. Phys.* **1940**, *8*, 212−224.
(28) Avrami, M. *J. Chem. Phys.* **1941**, *9*, 177−184.
(29) Ratkowski, D. *A non linear regression modelling*; Marcel Dekker: New York, 1983.
(30) Neutron and synchrotron radiation for condensed matter studies; Les éditions de physique; Springer-Verlag: New York, 1993; Vol. 1.
(31) Langford, J. I.; Louër, D. *Rep. Prog. Phys.* **1996**, *59*, 131−234.

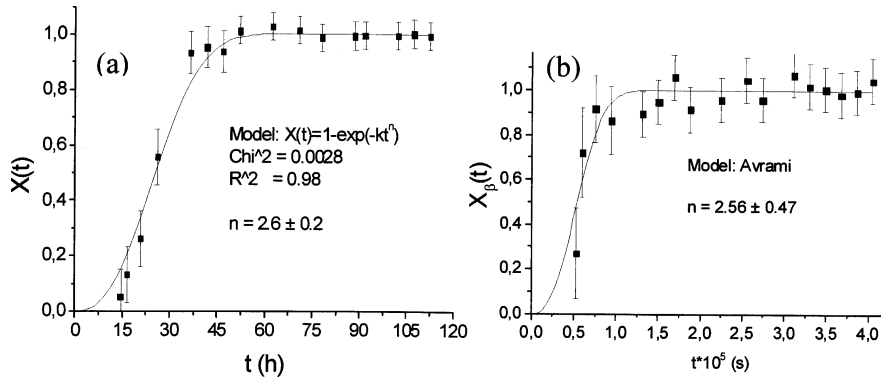

Figure 3. (a) Mean modeling of the evolution process of total gold volume. (b) Evolution of the mean volume of gold nanoparticles.

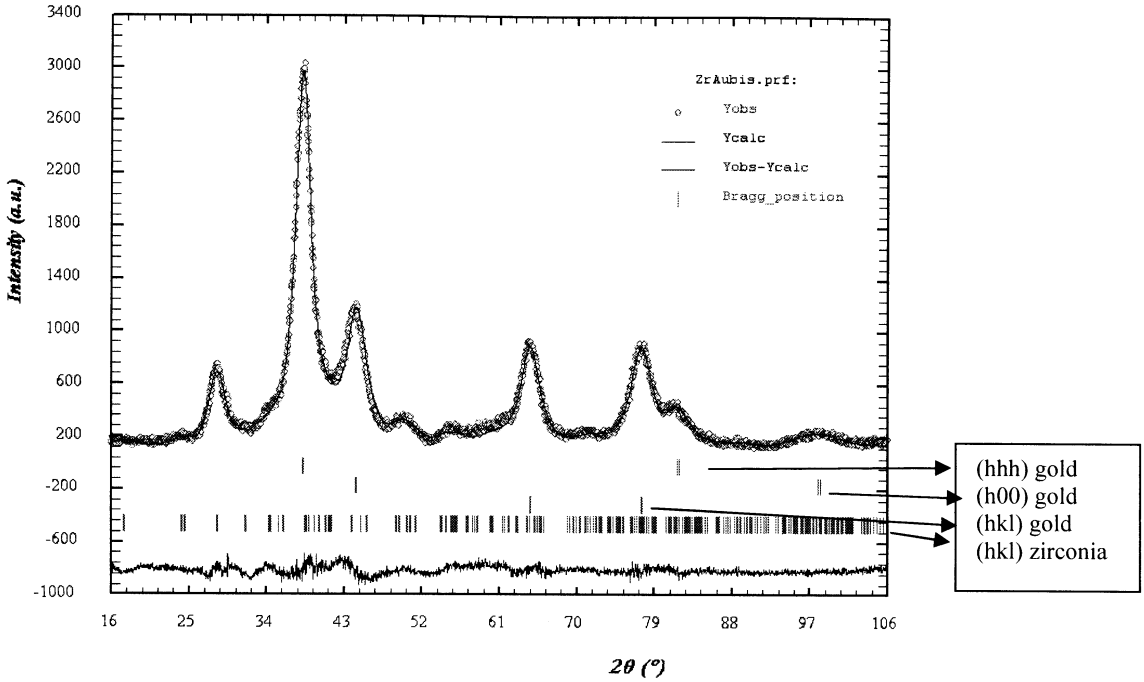

Figure 4. X-ray diffraction pattern on the sample after oxidation of ZrAu for 10 days. Observed profiles are plotted together with the calculated profile from the Rietveld refinement. Values of the refinement reliability factors: $R_p = 5.63\%$, $R_{wp} = 7.73\%$, $R_{exp} = 5.01\%$, and $\chi^2 = 2.38$. The sticks correspond to the three sets of reflections for gold and one set for zirconia.

Table 1. Values of the AEs Deduced from the Mean Analysis and from the log Plot of $X(t)$ and $X_\beta(t)$

$X(t)$	$X_\beta(t)$
$n = 2.6 \pm 0.2$	$n_\beta = 2.56 \pm 0.47$
$n_1 = 4 \pm 0.2$	$n_{\beta 1} = 2.9 \pm 1.5$
$n_2 = 0.67 \pm 0.06$	$n_{\beta 2} = 0.65 \pm 0.15$

plots can no longer be considered as asymptotes. From these observations we have calculated two different values for the AE as a function of time for each plot: n_1 and n_2 for the total volume evolution and $n_{\beta 1}$ and $n_{\beta 2}$ for the gold particles mean intrinsic volume evolution (Table 1). We can see that before t_0, values of n_1 and $n_{\beta 1}$ are quite different even if the error on the second value is rather large. On the contrary, after t_0, values of n_2 and $n_{\beta 2}$ are nearly equal.

Microstructural properties of final products (nanosized Au and ZrO_2 particles) from the X-ray diagram have been realized. To take into account the contribution of both nanosized phases simultaneously, a whole pattern fitting was performed using the Rietveld method. Indeed, the Bragg reflection intensities being constrained from the structural model, the contributions of each phase to the total diagram are correctly separated.

Furthermore, to extract microstructural information from the diffraction profiles, the instrumental resolution function was used to correct the observed profiles for the instrumental broadening.

For the gold phase, the standard face-centered cubic description was used, and for the monoclinic zirconia, the structural model of Wang et al.[32] was checked. As a result of very broad reflections, the atomic coordinates were not refined and only an overall atomic displacement parameter was adjusted with the scale factors and the profile shape parameters. Figure 4 shows the result of Rietveld adjustment performed on the pattern recorded after the oxidation for 10 days.

Preliminary refinement (with one set of reflections) showed that some gold Bragg reflections were not satisfactorily adjusted in terms of relative intensities and broadening. To obtain a better agreement between observed and calculated patterns, it was necessary to correct the intensities of the gold {*hhh*} family with a preferred orientation function. Despite the preferred orientation correction, the broadened

(32) Wang, J.; Li, H. P.; Stevens, R. *J. Mater. Sci.* **1992**, *27*, 5397−5430.

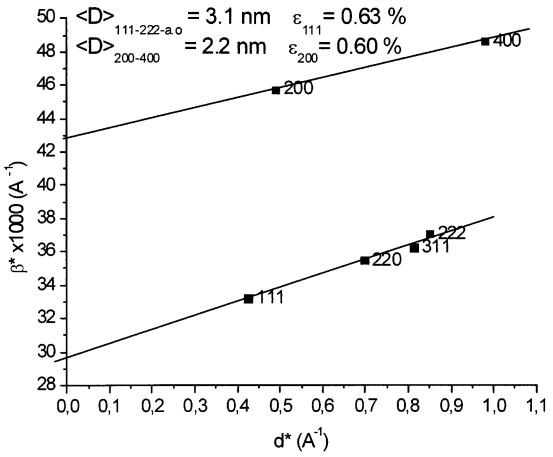

Figure 5. W−H plot for the sample reciprocal breadth as a function of the reciprocal interreticular distance d^*.

Table 2. Values of the Mean Apparent Size of Crystallites after 10 Days of Growth in Air and at Room Temperature

phase	mean size (nm)	phase	mean size (nm)
gold	$\langle D\rangle_{hhh} = 3.2 \pm 0.2$ $\langle D\rangle_{ao} = 3.0 \pm 0.2$ $\langle D\rangle_{h00} = 2.2 \pm 0.2$	zirconia	$\langle D\rangle = 3.6 \pm 0.3$

profiles of the gold $\{h00\}$ family were not properly refined. To take into account a possible anisotropic broadening of gold peaks, three sets of reflections were checked and independently fitted. The analysis of the zirconia phase is much more complex because of the weak intensity of the broadened diffraction peaks. Nevertheless, the intensities of the $\{\bar{h}hh\}$ zirconia family were also corrected with the preferred orientation function.

The mean size of diffracting domains along the various crystallographic directions has been determined from the Rietveld analysis (see Table 2) and confirms the crystal shape anisotropy predicted by the JMAK analysis.

For gold reflections, thanks to the Rietveld procedure, a microstrain analysis has also been performed. Indeed, from the observed profiles corrected for the instrumental broadening, it was possible to determine the apparent crystallite size and microstrains from the Williamson−Hall (W−H) plot[33] (Figure 5). This representation based on the plot of the intrinsic reciprocal integrated width, β^*, of diffraction peaks (depending on the Miller indices of the Bragg reflections) clearly shows a difference between the intercept at the origin of the line corresponding to the $\{h00\}$ family reflections and the other reflections. The intercept of the $\{h00\}$ family being greater than the others, it signifies that gold particles are smaller along the [100] direction. Slopes of the W−H plot are relevant to the microstrain rate (ϵ) present in particles.[32] It reveals that the mean value of microstrains along the $\{h00\}$ direction is approximately the same as along all the other directions.

After several weeks, the oxide layer is no longer compact and is reduced to the powder form. Size evolution of gold nanoparticles in this powder has been followed over 1 year at several time intervals by X-ray diffraction (Figure 6a). Each calculated size has been deduced from a Rietveld analysis performed on the different patterns. The time $t = 0$ months corresponds, in fact, to the end of the Avrami analysis, that is, after 10 days of exposure. We can see that crystallite dimensions evolve differently from each other along the several crystallographic directions. After 1 year, particle dimensions seem to be greater along the $\{hhh\}$ and $\{hh0\}$ directions and smaller along the 100 one.

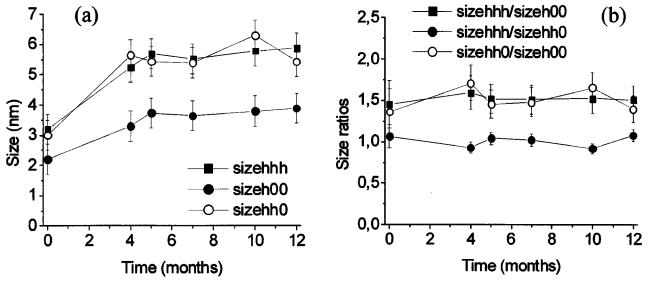

Figure 6. (a) Evolution of the different mean sizes of the gold particles along the three major crystallographic directions. (b) Evolutions of the different size ratios.

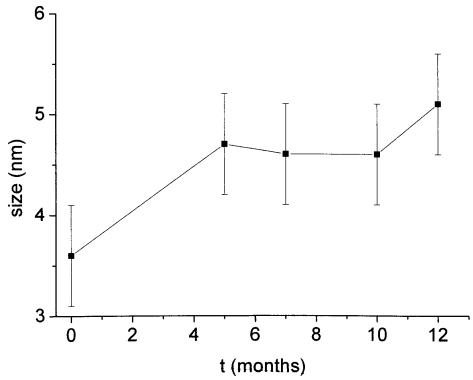

Figure 7. Evolution of size of zirconia nanoparticles over 1 year.

Concerning zirconia nanoparticle mean size evolution, we can see on Figure 7 a very slow evolution from 3−4 nm to 4−5 nm after 12 months.

TEM Observations. As a result of the very fast transformation kinetics, observation of the nucleation and growth of gold nanoparticles in the first step of their formation is impossible by this technique. As a result of the oxidation rate, at the end of the preparation procedure, alloy TEM samples are already oxidized and the beginning of the nucleation process is not observable. TEM was used to characterize particles after 11 months of aging in air and at room temperature. A statistical study of the mean size of particles is impossible because of the high state of agglomeration of observed aggregates. Only sides of these aggregates, or the thinnest ones, are observable. As a result of the high contrast of gold, we can easily distinguish approximately spherical gold particles (Figure 2a). This identification was verified by indexing Fourier transform (Figure 2b). The smaller and low contrasted particles correspond to ZrO_2 crystallites. Various Fourier transforms taken on these particles could all be indexed in the monoclinic phase of ZrO_2 (Figure 2c). On thinner agglomerates where the core of the nanocomposites is observable (Figure 2d), we can distinguish two populations of gold particles: the smallest ones are quasi spherical, and their mean size is about 5−10 nm; the second population concerns the biggest particles—they always exhibit a "dumbbell" shape.

(33) Hall, W. H. *Proc. Phys. Soc.* **1949**, *62*, 741−743.

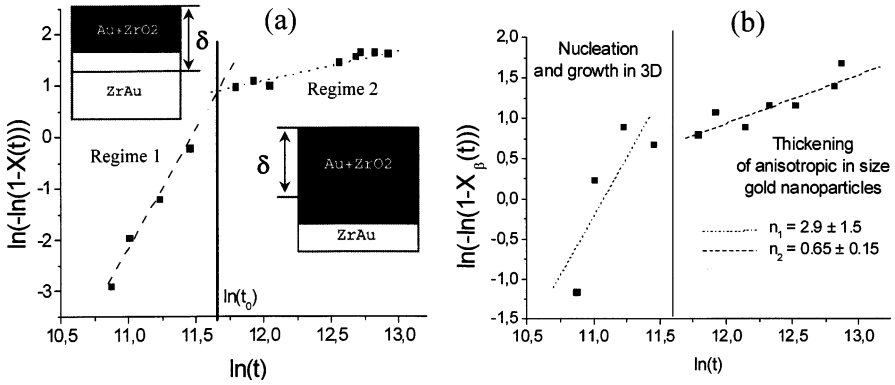

Figure 8. (a) Linear form plot of the JMAK equation. One can note two regimes in the evolution of the integrated intensity. (b) Refinement of the analysis of the growth process. In fact, the latter can be decomposed to two steps.

Zirconia nanoparticles are only observable on the sides of agglomerates (Figure 2f). We have noted that they always exhibit facetted morphology.

4. Discussion

Kinetics and Process of the Nucleation-Growth Phenomenon. The analysis of $X(t)$ and $X_\beta(t)$ following the JMAK model reveals the same mean AE for both evolutions. It could means that the first quantity evolution expresses the same overall process as the second: the growth of nanoparticles. From this value and the refinement of the Avrami theory, which has been done for many years,[22] we can conclude that the overall growth process is a three-dimensional one. Despite the fact that the evolution of $X(t)$ and $X_\beta(t)$ has been determined following only one crystallographic direction, this interpretation is in full accordance with TEM observations of the powder (three-dimensional gold nanoparticles).

Both parts observed on the Figure 8a,b can be related to the penetration depth of X-rays. According to the oxidation rate (80 nm·h^{-1}), at t_0, the thickness of surface layer is approximately equal to the value of the penetration depth (δ) of X-rays calculated from the absorption formula[34] for an incident angle $2\theta = 38°$ for the ZrO_2-Au composite. Consequently, before t_0, we still observe the oxidation interface instead of after.

When the calculated errors for $n_{\beta 1}$ and n_1 are taken into account, both are comparable. Moreover, when $t < t_0$, the increase of the total volume of gold can include several phenomena occurring in two different regions: at the oxidation front (nucleation of gold clusters) and in the surface layer [growth of clusters giving nanoparticles (coalescence, ostwald ripening, etc.)].

Consequently, it is difficult to draw a conclusion on the exact phenomenon describing the nucleation and growth of gold particles during the first part of $X_\beta(t)$ evolution. Nevertheless, we can conclude that it is a three-dimensional nucleation-growth process.

On the contrary, as n_2 and $n_{\beta 2}$ are equal, we can conclude that the increasing of the total volume of gold is due to the particle volume increase. Moreover, the value of $n_{\beta 2}$ could be related to a thickening of initial particles.[22,35−38] These initial particles would be the gold particles already formed in the first step (three-dimensional growth regime).

To sum up, an interpretation of the nucleation and growth mechanism from the AEs deduced from the $X(t)$ and $X_\beta(t)$ evolutions could be done: n_1, $n_{\beta 1} = 3-4$, nucleation and formation of gold clusters in three dimensions; n_2, $n_{\beta 2} = 0.7$, thickening of previous nucleated particles.

Over 1 year in air and at room temperature, the mean size of gold and zirconia nanoparticles increased slightly.

Concerning gold nanoparticles, after 10 days of air exposure and over 1 year, the mean size continues to increase. Ratios between sizes calculated following different crystallographic directions (Figure 6b) are constant. It means that gold nanoparticles continue to grow in the same way in all directions and confirms, at a larger time scale, the thickening process deduced from the Avrami analysis (n_2 and $n_{\beta 2}$). Moreover, we can see on Figure 9 that this evolution over 1 year is well-defined by a classical grain growth model[47−49]

$$D = kt^a$$

where D is mean size of particles, k is the time constant, t is the time, and a is the characteristic exponent.

In a pure single-phase system, the a exponent would be equal to 0.5.[49] Grey and Higgins showed that the introduction of impurities induces a diminution of this value. This effect is due to the variations of the mobility of grains caused by the presence of these impurities, the limited grain size defined

(34) Guinier, A. Théorie et technique de la radiocristallographie. Dunod: 1964.
(35) Doremus, R. H. *Acta Metall.* **1957**, *5*, 393.
(36) Wert, C.; Zener, C. *J. Appl. Phys.* **1950**, *21*, 5.
(37) Ham, F. S. *J. Phys. Chem. Solids* **1958**, *6*, 335.
(38) Ham, F. S. *J. Appl. Phys.* **1959**, *30*, 915.
(39) Wolf, D.; Lutsko, J. F. *Phys. Rev. Lett.* **1988**, *60*, 1170.
(40) Cammarata, R.; Sieradzki, K. *Phys. Rev. Lett.* **1989**, *62*, 2005.
(41) Edelstein, A. S.; Cammarata, R. C. *Nanomaterials: Synthesis, Properties*. Shim, J. H.; Lee, B. J.; Cho, Y. W. *Surf. Sci.* **2002**, *512*, 262−268.
(42) Nieman, G. W.; Weertman, J. R.; Siegel, R. W. *J. Mater. Res.* **1991**, *6*, 1012.
(43) Eckert, J.; Holzer, J. C.; Krill, C. E.; Johnson, W. L. *J. Mater. Res.* **1992**, *7*, 1751.
(44) Parise, M.; Touet, I.; Sicardy, O. *Textures Microstruct.* **1998**, *30*, 247−263.
(45) Parise, M.; Scardy, O.; Cailletaud, G. *J. Nucl. Mater.* **1998**, *256*, 35−46.
(46) Petigny, N.; Barberis, P.; Lemaignan, C.; Valot, Ch.; Lallemant, M. *J. Nucl. Mater.* **2000**, *280*, 318−330.
(47) Hillert, M. *Acta Metall.* **1965**, *13*, 227.
(48) Grey, E. A.; Higgins, G. T. *Acta Metall.* **1973**, *21*, 309.
(49) Hu, H. *Can. Metall. Q.* **1974**, *13*, 275.

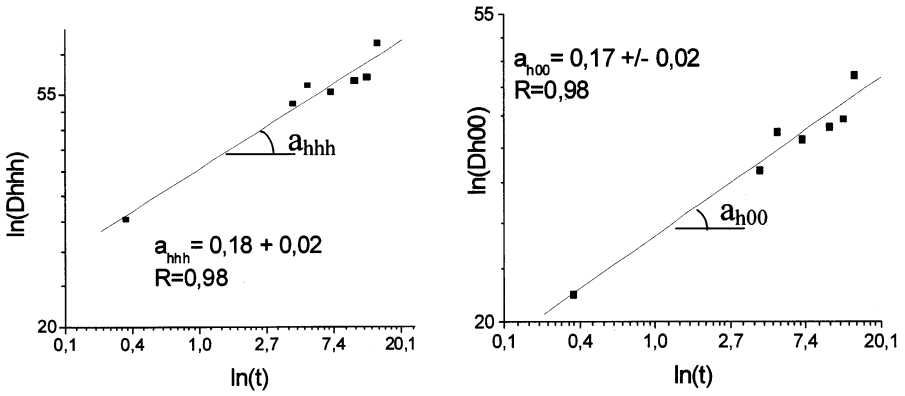

Figure 9. Evolution of size of gold nanoparticles over 1 year (logarithmic scale). We can see that both evolutions can be fitted with straight lines in which the slope is equal to the exponent *a*.

by the thermodynamic conditions of the experience, and the "morphology" of the sample (diminution of grain boundaries amounted with particle growth, etc.).[48]

The exponent *a* has been calculated for each evolution. All values are lower than 0.5. In our system, even if zirconia cannot be considered as an impurity because of its molar fraction, it modifies the gold nanoparticle mobility and could explain the lowest values of the *a* parameter, following Grey and Higgins' work. Close values of a_{hhh} and a_{h00} indicates the same growth process in both directions, and are consistent with the thickening behavior predicted by the size ratio evolution over 1 year and by the Avrami analysis.

However, the growth mechanism extrapolated from these mathematical analyses needed to be improved. TEM observations, performed 11 months after the beginning of the aging process, can lead to a determination of the long range of the time growth phenomenon. As mentioned above, the particles can be separated in two groups, spherical and "dumbbell" shaped. Because a dumbbell shape is characteristic of the impingement of two spherical particles,[50] we can consider that the ovoid particle morphology observed is relevant to a coalescence mechanism between two spherical particles and occurring at the time of the observation as that seen in Figure 2e. Thus, we can say that one of the growth processes deduced from Avrami analysis (thickening) occurred by the way of the coalescence of particles. However, an Ostwald ripening type mechanism cannot be ignored. Indeed, some small gold particles are very close to bigger ones (Figure 2d).

Microstructural Analysis. Ten days after the beginning of the oxidation process, Rietveld analysis revealed a slightly different particle size following the [*h*00] crystallographic direction (Table 2) compared to the other direction. However, no proof by direct observation of this phenomenon can be given. A W−H analysis of diffraction diagrams allows us to determine the mean amount of microstrains present in these nanoparticles. Microstrains are a natural component of nanostructured materials and are mainly due to the large number of interfaces and grain boundaries.[39−41] Calculated values for these microstrains are nearly equal in all directions and are consistent with the microstrain rates usually found in metallic nanoparticles.[42,43]

As in the case of gold nanoparticles, a large preferred orientation of zirconia particles along the $\{\bar{h}hh\}$ direction was observed. Concerning the zirconium, this phenomenon has been previously observed during the oxidation of zirconium alloys used in nuclear reactors (Zircaloy).[44−46] The preferred orientation of both products leads us to think that the composite zirconia−gold exhibits a kind of slight "self-orientation" during its growth probably induced by the starting ZrAu alloy.

5. Conclusion

Spontaneous oxidation in air and at room temperature of the ZrAu alloy is a selective oxidation type. This phenomenon involves the segregation of gold atoms. The X-ray and TEM combined analyses of the growth kinetics of gold nanoparticles (X-ray diffraction) and of the microstructure (X-ray diffraction and TEM) allow us to say that the oxide layer is a close mixture of gold and zirconia nanoparticles. The stability of these gold nanoparticles has been studied over 1 year from their formation in air and at room temperature.

At the early stages of oxidation, it has been shown that the growth process could be mainly described with a JMAK model with an exponent $n = 2.6$. This value seems indicate a three-dimensional growth process. It has also been shown that this main process could be decomposed to two parts: At the beginning, gold clusters nucleate and grow by the way of a three-dimensional mechanism. Avrami analysis of the evolution of the gold fraction transformed completed with TEM observations have shown that the growth process after nucleation is due to coalescence and Ostwald ripening mechanisms.

The microstructural analysis of the reaction products after 10 days of oxidation reveals that this process leads to the formation of gold and zirconia nanoparticles of about 3−4 nm in diameter. Rietveld analysis of X-ray diffraction patterns reveals that gold particles exhibit a slight anisotropy of size along the [*h*00] direction.

Moreover, gold nanoparticles continue to grow at room temperature. X-ray analysis over 1 year confirms the anisotropy of the particles. This long range of time for the growth process allowed the non-asymptotic behavior of the

(50) Fluëli, M.; Buffat, P. A.; Borel, J.-P. *Surf. Sci.* **1988**, *202*, 343.

linear form of the Avrami analysis to be validated. After 1 year, the gold crystallite mean size is about 5−6 nm. Over this period, the growth mechanism seems to be in good accordance with the model proposed by Hillert.[47] The relatively slow growth rate allows stabilizing very fine particles at room temperature during a long time.

As far as the future is concerned, the reproducibility of this amazing phenomenon could be studied by substituting gold and/or zirconium to synthesize a ternary or quaternary composite metal oxide for various applications such as catalytic gas sensors.

CM040187J